On the lattice Boltzmann method for multiphase flows

By S. H. Kim AND H. Pitsch

1. Motivation and objectives

The lattice Boltzmann (LB) method (McNamara & Zanetti 1988; Qian *et al.* 1992; Chen & Doolen 1998; Benzi *et al.* 1992; Succi 2001) is a reduced-order kinetic model to reproduce the Navier-Stokes hydrodynamics (and beyond) at a macroscopic level. Since the pioneering work of McNamura and Zanetti (1988), the LB method has been extended to various complex flows involving, for example, multicomponent and interfacial phenomena, and has been particularly successful for multiphase flows in complex geometry and porous media (Succi 2001; Chen & Doolen 1998). However, in computation of multiphase flows, its application range has been limited because of numerical instability, especially for flows with large density ratio between different phases. The objective of this study is to develop a more stable and efficient LB method for multiphase flows with large density ratios.

Most multiphase LB methods that have been developed so far (Chen & Doolen 1998; Shan & Chen 1993; Swift *et al.* 1996; He *et al.* 1997) belong to a class of the diffuse interface model (Jacqmin 1999), although with some exceptions (Shan & Chen 1993), in that an interface is numerically resolved with a few grid points across it. A specific formulation of the discrete kinetic model can be derived from a continuum kinetic equation such as the Enskog equation or can be constructed *a posteriori* in such a way that the corresponding macroscopic equation follows a desired hydrodynamic equation for multiphase flows. The former approach includes the model of Luo and Girimaji (2003) and of He *et al.* (1997), while the latter includes the Shan-Chen model (Shan & Chen 1993) and the free energy model (Swift *et al.* 1996). Typically, the density ratio that can be simulated by these methods is restricted to $O(10)$.

Several approaches have been developed to resolve the large density ratio problem in the LB method (Inamuro *et al.* 2004; Lee & Lin 2005; Zheng *et al.* 2006). Of these remedies, all the existing methods that can simulate density ratios up to $O(1000)$ are based on the use of the order parameter to describe the interface dynamics. Based on the free energy LB method, Inamuro *et al.* (2004) employed the projection method for which the pressure Poisson equation is solved at each time step to enforce the divergence-free condition for the velocity field. Lee and Lin (2005) proposed a stable discretization scheme for the mean-field LB method of He *et al.* (1999). Zheng *et al.* (2006) proposed an LB method that reproduces the Cahn-Hillard equation for the order parameter. The nominal density is, however, used for the continuity and momentum equations and thus does not correctly describe the momentum transport in flows with large density ratios in the model of Zheng *et al.* (2006).

In this paper, we develop a lattice Boltzmann method that reproduces the phase-field model (Jacqmin 1999) for macroscopic hydrodynamics. Two formulations of the LB method are presented. A hybrid LB-finite difference method is also proposed. One of

origins of the large density ratio problem in the LB method is discussed, and the results for validation studies are presented.

2. Phase-field lattice Boltzmann method

2.1. *Interface dynamics in the phase-field method*

In the phase-field method, The dynamics of interfaces between different phases are described using the order parameter C. The order-parameter is an indicator of different phases, and varies smoothly in an interfacial region. In incompressible flows, the order-parameter is typically given as a function of the density and, here, defined by

$$C = f(\rho) = \frac{\rho - \rho_l}{\rho_h - \rho_l}, \tag{2.1}$$

where ρ_h and ρ_l are the density of heavier and of lighter fluid, respectively. The evolution of C is described by the Cahn-Hillard equation (Jacqmin 1999), which can be written as

$$\frac{\partial C}{\partial t} + u_\alpha \frac{\partial C}{\partial x_\alpha} = \frac{\partial}{\partial x_\alpha}\left(M \frac{\partial \phi}{\partial x_\alpha} \right), \tag{2.2}$$

where M is the mobility. The chemical potential, ϕ, is given by

$$\phi = \frac{\delta \Phi}{\delta C} = a\epsilon\sigma\nabla^2 C + a\epsilon^{-1}\sigma\Psi'(C). \tag{2.3}$$

The free energy for isothermal fluid, Φ, can be written as

$$\Phi = \frac{1}{2} a\epsilon\sigma|\nabla C|^2 + a\epsilon^{-1}\sigma\Psi(C). \tag{2.4}$$

The following form of the bulk free energy is used here:

$$\Psi(C) = \frac{1}{4} C^2(1-C)^2. \tag{2.5}$$

The surface tension for a planar interface is given by

$$\sigma = a\epsilon\sigma \int_{-\infty}^{\infty} \left(\frac{\partial C}{\partial n} \right)^2 dn, \tag{2.6}$$

where n is the coordinate in the direction normal to an interface. This gives $a = 6\sqrt{2}$. The thickness of the interface is of the order of ϵ.

The flow field is described by

$$\frac{\partial u_\alpha}{\partial x_\alpha} = 0, \tag{2.7}$$

$$\rho\left(\frac{\partial u_\alpha}{\partial t} + u_\alpha \frac{\partial u_\beta}{\partial x_\beta} \right) = -\frac{\partial p}{\partial x_\alpha} + \frac{\partial}{\partial x_\beta}\left[\rho\nu \left(\frac{\partial u_\beta}{\partial x_\alpha} + \frac{\partial u_\alpha}{\partial x_\beta} \right) \right] + \rho F_\alpha^s. \tag{2.8}$$

The surface tension force F_α^s can be implemented in different ways, and the difference between the different implementation of the surface tension can be absorbed into the "pseudo pressure," p, in the momentum equation. Here, the stress form of the surface tension is used, which is given by

$$F_\alpha^s = \frac{1}{\rho}\frac{\partial}{\partial x_\beta}\left(\frac{\partial^2 \phi}{\frac{\partial \phi}{\partial x_\alpha \partial x_\beta} - \partial x_\gamma \partial x_\gamma} \delta_{\alpha\beta} \right). \tag{2.9}$$

The pseudo pressure p for the stress form of the surface tension force is the hydrodynamic pressure P.

2.2. *Lattice Boltzmann method*

Here, two LB methods that reproduce Eqs. (2.2), (2.7), and (2.8) for macroscopic hydrodynamics are presented.

2.2.1. *Momentum-based formulation*

The discrete velocity equations (DVEs) for the phase-field model can be written as

$$\frac{\partial f_i}{\partial t} + c_{i\alpha}\frac{\partial f_i}{\partial x_\alpha} = -\frac{1}{\tau}(f_i - f_i^{\mathrm{e}}) + \frac{c_{i\alpha} - u_\alpha}{c_s^2}\frac{\partial(\rho c_s^2 - p)}{\partial x_\alpha}\Gamma_i + \Psi_{i\alpha}\rho F^s, \tag{2.10}$$

$$\frac{\partial g_i}{\partial t} + c_{i\alpha}\frac{\partial g_i}{\partial x_\alpha} = -\frac{1}{\tau}(g_i - g_i^{\mathrm{e}}) + \Psi_{i\alpha}\left(F_\alpha^s - F_\alpha^p\right), \tag{2.11}$$

where

$$\Psi_{i\alpha} = w_i\left[\frac{(c_{i\alpha} - u_\alpha)}{c_s^2} - \frac{u_\beta c_{i\alpha}c_{i\beta}}{c_s^4}\right], \tag{2.12}$$

$$\Gamma_i = \frac{c_{i\alpha}u_\alpha}{c_s^2} + \frac{(c_{i\alpha}c_{i\beta} - c_s^2\delta_{\alpha\beta})u_\alpha u_\beta}{2c_s^4}, \tag{2.13}$$

$$F_\alpha^p = -\frac{\partial p}{\partial x_\alpha}. \tag{2.14}$$

$c_{i\alpha}$ is the discrete velocity for the distribution functions f_i and g_i. The DVE for the distribution function f_i describes the mass and momentum conservation, while that for g_i describes the evolution of the order-parameter. The equilibrium functions are given by

$$f_i^{\mathrm{e}} = w_i\left[\frac{p}{c_s^2} + \rho\left(\frac{c_{i\alpha}u_\alpha}{c_s^2} + \frac{(c_{i\alpha}c_{i\beta} - c_s^2\delta_{\alpha\beta})u_\alpha u_\beta}{2c_s^4}\right)\right] \tag{2.15}$$

$$g_i^e = w_i^0\phi + w_i\left[\frac{\phi u_\alpha c_{i\alpha}}{c_s^2} + G_{i\alpha\beta}\left(m\phi\delta_{\alpha\beta} + Cu_\alpha u_\beta\right)\right], \tag{2.16}$$

where

$$G_{i\alpha\beta} = w_i\frac{c_{i\alpha}c_{i\beta} - c_s^2\delta_{\alpha\beta}}{2c_s^4} \tag{2.17}$$

$$w_0^0 = 1, w_i^0 = 0 (i \neq 1). \tag{2.18}$$

The lower moments of f_i and g_i are

$$\sum f_i = p, \tag{2.19}$$

$$\sum c_{i\alpha}f_i = \rho u_\alpha, \tag{2.20}$$

$$\sum g_i = C. \tag{2.21}$$

The LB equation can be obtained by the spatial and time integration of the DVB equation. The second-order integration along a discrete velocity gives

$$f_i(\mathbf{x} + \mathbf{c}_i\delta t, t + \delta t) - f_i(\mathbf{x}, t) = -\frac{1}{\tau/\delta t + 0.5}(f_i - f_i^{\mathrm{e}}) + \frac{\tau}{\tau + 0.5\delta t}\delta t\Psi_{i\alpha}\left(F_i^s + F_i^p\right). \tag{2.22}$$

The spatial derivatives in the LB equations can be evaluated using the isotropic discretization. The Taylor expansion of ϕ can be written as

$$\phi(\mathbf{x}+\delta t\mathbf{c}_i)=\phi(\mathbf{x})+\delta t c_{i\alpha}\frac{\partial\phi}{\partial x_\alpha}+\frac{1}{2}\delta t^2 c_{i\alpha}c_{i\beta}\frac{\partial^2\phi}{\partial x_\alpha x_\beta}+O(\delta t^3). \tag{2.23}$$

From the isotropy of the quadrature, the first-order derivatives and Laplacian can be evaluated by

$$\frac{\partial\phi}{\partial x_\alpha}\approx\frac{1}{c_s^2\delta t}\sum w_i c_{i\alpha}\phi(\mathbf{x}+\mathbf{c}_i\delta t), \tag{2.24}$$

$$\frac{\partial^2\phi}{\partial x_\alpha^2}\approx\frac{2}{c_s^2\delta t^2}\sum w_i\left[\phi(\mathbf{x}+\mathbf{c}_i\delta t)-\phi(\mathbf{x})\right]. \tag{2.25}$$

Note that the discretization scheme in Pooley & Furtado (2008), which is shown to reduce the spurius currents, is identical to the above.

2.3. *Velocity-based formulation*

In this formulation, the equilibrium function is based on the velocity u_α, not the momentum ρu_α. The DVB equation can be written as

$$\frac{\partial f_i}{\partial t}+c_{i\alpha}\frac{\partial f_i}{\partial x_\alpha}=-\frac{1}{\tau}(f_i-f_i^{\mathrm{e}})+\Psi_{i\alpha}\left(F_\alpha^s+F_\alpha^p+F_\alpha^v\right)+w_i^0F^d, \tag{2.26}$$

where

$$f_i^{\mathrm{e}}=w_i^0\frac{p}{c_s^2}+w_i\left(\frac{c_{i\alpha}u_\alpha}{c_s^2}+\frac{(c_{i\alpha}c_{i\beta}-c_s^2\delta_{\alpha\beta})u_\alpha u_\beta}{2c_s^4}\right) \tag{2.27}$$

$$F_\alpha^p=-\frac{1}{\rho}\frac{\partial p}{\partial x_\alpha} \tag{2.28}$$

$$F_\alpha^v=-\frac{\nu}{\rho}\frac{\partial\rho}{\partial x_\beta}\left(\frac{\partial u_\beta}{\partial x_\alpha}+\frac{\partial u_\alpha}{\partial x_\beta}\right) \tag{2.29}$$

$$F^d=-c_d(\rho-1)\frac{\partial u_\gamma}{\partial x_\gamma}. \tag{2.30}$$

The second-order integration along a discrete velocity gives

$$\begin{aligned}f_i(\mathbf{x}+\mathbf{c}_i\delta t,t+\delta t)-f_i(\mathbf{x},t)=&-\frac{1}{\tau/\delta t+0.5}(f_i-f_i^{\mathrm{e}})\\&+\frac{\tau}{\tau+0.5\delta t}\delta t\left[\Psi_{i\alpha}\left(F_\alpha^s+F_\alpha^p+F_\alpha^v\right)+w_i^0F^d\right],\end{aligned} \tag{2.31}$$

The velocity and pressure are obtained by

$$u_\alpha=\sum c_{i\alpha}f_i+\frac{\delta t}{2}\left(\frac{F_\alpha^s}{\rho}+F_\alpha^p+F_\alpha^u\right). \tag{2.32}$$

$$p=c_s^2\sum f_i+\frac{\delta t}{2}F^d. \tag{2.33}$$

In order to solve the coupled equations for the pressure and velocity in Eqs. (2.32) and (2.33), the predictor-corrector step is employed. At the predictor step,

$$p^*=c_s^2\sum f_i^{(n)}+\frac{\delta t}{2}F^{d(n-1)}, \tag{2.34}$$

$$u_\alpha^* = \sum c_{i\alpha} f_i^{(n)} + \frac{\delta t}{2}\left(F^{s(n)} + F^{p(*)} + F^{v(n-1)}\right). \tag{2.35}$$

At the corrector step,

$$p^{(n)} = c_s^2 \sum f_i^{(n)} + \frac{\delta t}{2} F^{d(*)}, \tag{2.36}$$

$$u_\alpha^{(n)} = \sum c_{i\alpha} f_i^{(n)} + \frac{\delta t}{2}\left(F^{s(n)} + F^{p(n)} + F^{v(*)}\right). \tag{2.37}$$

Before evaluating the moments, a filtering operation is applied to the pressure field to enhance the numerical stability. The second-order filtering operation used here is

$$\tilde{\phi}(\mathbf{x}) = \sum w_i \phi(\mathbf{x} + \mathbf{c}_i \delta t). \tag{2.38}$$

Higher-order filters (Ricot *et al.* 2009) are given by

$$\tilde{\phi}(\mathbf{x}) = \phi(\mathbf{x}) - a \sum_{j=1}^{D} \sum_{m=-M}^{M} d_m \phi(\mathbf{x} + \mathbf{x}_j), \tag{2.39}$$

where $\mathbf{x}_j$ is the unit vector in the j-direction, and D is the dimensionality of the problem. The coefficients for the fifth-order filter are $d_0 = 6/16$, $d_1 = -4/16$, and $d_2 = 1/16$, while those for the seventh-order filter are $d_0 = 5/16$, $d_1 = -15/64$, $d_2 = 2/32$, and $d_3 = -1/64$. Because the filtering operation is applied only to the pressure field, it smoothes out high-frequency oscillations only for the pressure field and does not directly affect the velocity field and viscous dissipation.

2.4. *Hybrid LB-finite-difference method*

In this method, the velocity and pressure fields are solved using the lattice Boltzmann method, while the order parameter is solved using the finite difference method. The velocity-based formulation, vLBM, is used to solve the flow field. The order parameter is obtained by

$$\frac{C^{(n+1)} - C^{(n)}}{\delta t} = \nabla_d \cdot \left(M \nabla_d \phi^{(n+1/2)}\right) - \mathbf{u}^{(n+1/2)} \cdot \nabla_d C^{(n+1/2)}, \tag{2.40}$$

where $C^{(n+1/2} = 1.5C^{(n)} - 0.5C^{(n-1)}$ and $\mathbf{u}^{(n+1/2)} = 1.5\mathbf{u}^{(n)} - 0.5\mathbf{u}^{(n-1)}$. The second-order TVD scheme (van Leer 1979) is used for the convective operator, while the second-order central difference scheme is used for the chemical potential term.

3. Results and discussion

3.1. *Continuity*

In this section, the LB formulation for which the equilibrium function is based on the momentum ρu_i, rather than the velocity u_i, is shown not to satisfy the continuity equation. An implication of this finding on other LB methods is discussed.

As an example, results for a single bubble rising in viscous fluid are shown in Fig. 1. The density ratio ρ_h/ρ_l is 100. For the momentum-based formulation, mLBM, the error in the divergence field is much higher than the truncation error in the asymptotic expansion of the LB equation, $O(\mathrm{Ma}^2)$. The divergence error for the velocity-based formulation, vLBM, however, is within the truncation error of the LB method. For incompressible flow simulations, the LB method can be regarded as an artificial compressibility method. The divergence error for vLBM depends on c_d. The sound speed in vLBM is $\sqrt{c_{vp} c_s (\rho + 1)}$.

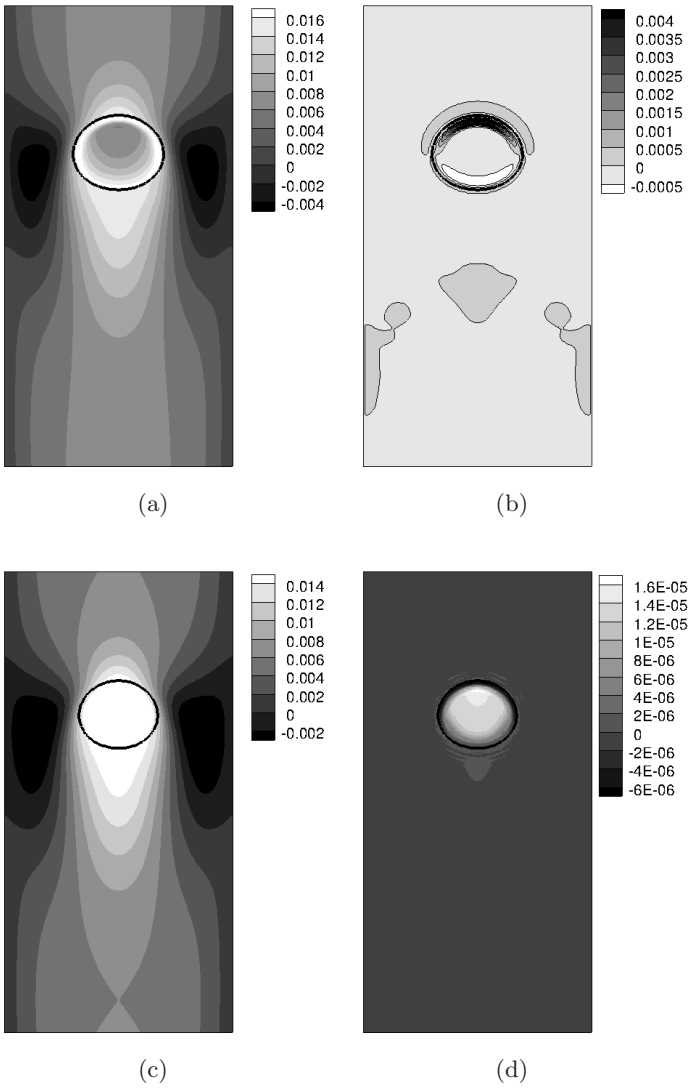

FIGURE 1. Axial velocity and divergence fields for a bubble rising in a viscous fluid. (a) axial velocity predicted by mLBM; (b) divergence predicted by mLBM; (c) axial velocity predicted by vLBM; (d) divergence predicted by vLBM. The thick solid line represents a bubble.

Increasing c_d, therefore, lowers an error in the divergence field. The value of c_d used for the results in Fig. 1 is 6.

To illustrate the major sources of the continuity error in the momentum-based formulation, mLBM, a special case of $\tau/\delta t = 0.5$ is considered. When $\tau/\delta t = 0.5$, the equation for mLBM can be written as

$$f_i(\mathbf{x}, t) = f_i^{\mathrm{e}}(\mathbf{x} - \mathbf{c}_i\delta t, t - \delta t) + \frac{1}{2}\delta t F_i(\mathbf{x} - \mathbf{c}_i\delta t, t - \delta t). \tag{3.1}$$

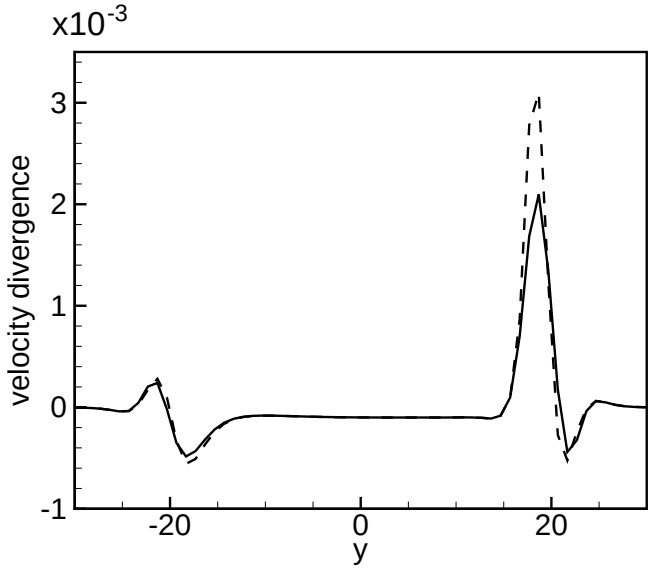

FIGURE 2. Divergence of the velocity field along the center of a bubble, predicted by mLBM (solid line: $\delta u_\alpha/\delta x_\alpha$, dashed line: $\left(\delta\rho u_\alpha/\delta x_\alpha - u_\alpha \delta\rho/\delta x_\alpha\right)/\rho$).

$$f_i(\mathbf{x},t) - f_i(\mathbf{x},t-\delta t) = f_i^{\mathrm{e}}(\mathbf{x}-\mathbf{c}_i\delta t, t-\delta t) - f_i(\mathbf{x},t-\delta t) + \frac{1}{2}\delta t F_i(\mathbf{x},t-\delta t) + \frac{1}{2}\delta t\left[F_i(\mathbf{x}-\mathbf{c}_i\delta t, t-\delta t) - F_i(\mathbf{x},t-\delta t)\right]. \tag{3.2}$$

From this, the semi-discrete form of the leading-order continuity equation can be obtained:

$$\frac{\partial p}{\partial t} = \frac{\delta \rho u_\beta}{\delta x_\beta} - u_\beta \frac{\delta \rho}{\delta x_\beta} + O(\delta t), \tag{3.3}$$

where the discrete operator, $\delta\phi/\delta x_\alpha$, is defined by Eq. (2.24). To obtain the correct discrete continuity equation requires

$$\rho \frac{\delta u_\beta}{\delta x_\beta} \approx \frac{\delta \rho u_\beta}{\delta x_\beta} - u_\beta \frac{\delta \rho}{\delta x_\beta}. \tag{3.4}$$

This discrete chain rule is not satisfied for the discrete operator given in Eq. (2.24), as shown in Fig. 2.

This analysis is related to the specific formulation of mLBM, including He *et al.* (1999) and Lee and Lin (2005). However, the violation of the discrete chain rule results in similar errors for most multiphase LB models. For example, a chain rule used when deriving the viscous term is also not satisfied discretely, which can result in the error in momentum conservation. The origin of this error is that the leading-order contribution in the hydrodynamic equations for the momentum-based formulation is obtained by the subtraction of two large terms, when the density ratio is large. In Eq. (3.4), the absolute values of two terms on the r.h.s. are much larger than the term on the l.h.s., when ρ_h/ρ_l is of $O(100)$ or larger.

ϵ	No filter	F1	F2($a = 0.25$)	F2($a = 0.5$)	F3 ($a = 0.25$)	F3 ($a = 0.5$)
0.6	2.1405E-005	3.6645E-005	2.1949E-005	2.2306E-005	2.1784E-005	2.1993E-005
0.8	6.4890E-006	2.2998E-005	6.5614E-006	6.7915E-006	6.4396E-006	6.5007E-006
1.0	2.5559E-006	1.6466E-005	2.5903E-006	2.7381E-006	2.5144E-006	2.5220E-006
1.2	1.1109E-006	1.2697E-005	1.1590E-006	1.2596E-006	1.1055E-006	1.1071E-006

TABLE 1. Maximum spurious velocity in a static drop (F1: Eq. (2.38), F2: fifth-order filter, F3: seventh-order filter).

ϵ	No filter	F1	F2($a = 0.25$)	F2($a = 0.5$)	F3 ($a = 0.25$)	F3 ($a = 0.5$)
0.8	Unstable	5.4244E-003	5.4171E-003	5.4160E-003	5.4189E-003	5.4186E-003

TABLE 2. Rising velocity of a single bubble (F1: Eq. (2.38), F2: fifth-order filter, F3: seventh-order filter).

3.2. *Effects of filtering*

In this section, the effects of filtering are investigated for static drop and rising bubble cases. For a static drop, the velocity vanishes. However, numerical simulations generate non-zero velocity because of imbalance in forces. This spurious velocity is observed in almost all numerical methods for interfacial flows. In Table 1 the spurious velocities are shown for different interface thicknesses and filters. The droplet radius is 20, the density ratio is 100, the viscosity ratio is 100, and the surface tension coefficient σ is 1. For $\epsilon = 0.6$, the effects of filtering on the spurious velocities are minor, while for $\epsilon > 1$, the magnitude of the spurious velocity for the second-order filter, F2, is an order of magnitude larger than that for no filtering. The higher-order filters, however, have little influence on the spurious velocity for all interface widths tested here.

Table 2 shows the rising velocity of a single bubble in viscous fluid, predicted using different filters. The density ratio ρ_h/ρ_l is 1000 and the viscosity ratio μ_h/μ_l is 100. The computational domain is discretized into 256×128 lattices. Without filtering, the computation is unstable. The rising velocity of the bubble predicted by different filters is almost identical. The effects of filtering on the flow field are negligible for this case.

3.3. *Capillary wave*

The capillary wave between two fluids is considered. In the long wavelength limit, an analytic solution exists. The decay rate and the oscillating frequency depend on the density ratio ρ_h/ρ_l, the surface tension σ, the kinematic viscosity ν, and the wave number of the initial perturbation k and, in the unit of $k^{3/2}\sqrt{\sigma(\rho_h + \rho_l)}$, given by the real and imaginary parts of

$$n = \frac{y^2 - 1}{\sqrt{s}}, \tag{3.5}$$

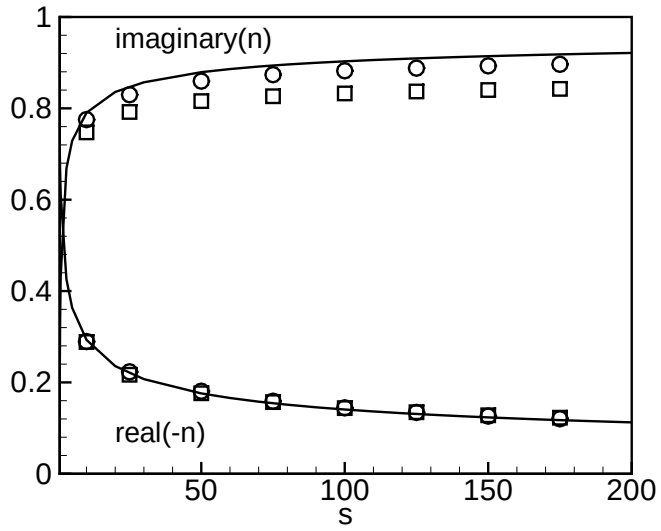

FIGURE 3. The oscillation frequency and the decay rate of the planar capillary wave (lines: linear theory, squares: LBM with 64×64 lattices, circles: LBM with 256×256 lattices).

where

$$s = \frac{\sigma}{k(\rho_h + \rho_l)\nu^2}. \tag{3.6}$$

y satisfies

$$y^4 + 4\alpha_1\alpha_2 y^3 + 2(1 - 6\alpha_1\alpha_2)y^2 - 4(1 - 3\alpha_1\alpha_2)y + (1 - 4\alpha_1\alpha_2) + s = 0, \tag{3.7}$$

where $\alpha_1 = \rho_h/(\rho_h + \rho_l)$ and $\alpha_2 = \rho_l/(\rho_h + \rho_l)$.

Figure 3 shows the oscillating frequency and the decay rate of the planar capillary wave. The Atwood number, $(\rho_h - \rho_l)/(\rho_h + \rho_l)$, is 0.5. The initial profile for the order parameter is given by

$$C = 0.5\left[1 + \tanh\left(\frac{y - L_y/2 + a_0\cos(2\pi x/\lambda)}{2\sqrt{2}\epsilon}\right)\right], \tag{3.8}$$

where a_0 and λ are the amplitude and the wavelength of the initial perturbation, respectively. The simulation is performed using the hybrid LB-finite-difference method. The LB method well predicts the decay rate for both resolutions, 64×64 and 256×256. However, the oscillating frequency is underpredicted, especially for 64×64 lattices. This underprediction of the oscillating frequency is also observed in Zhang *et al.* (2000), but the present results are in better agreement with the theory than are those in Zhang *et al.* (2000).

3.4. *Rayleigh-Taylor instability*

A Rayleigh-Taylor instability case is also simulated here using the hybrid LB-finite-difference method. The initial profile of the interface is given by

$$C = 0.5\left[1 + \tanh\left(\frac{y - L_y/2 + a_0\cos(2\pi x/L_x)}{2\sqrt{2}\epsilon}\right)\right], \tag{3.9}$$

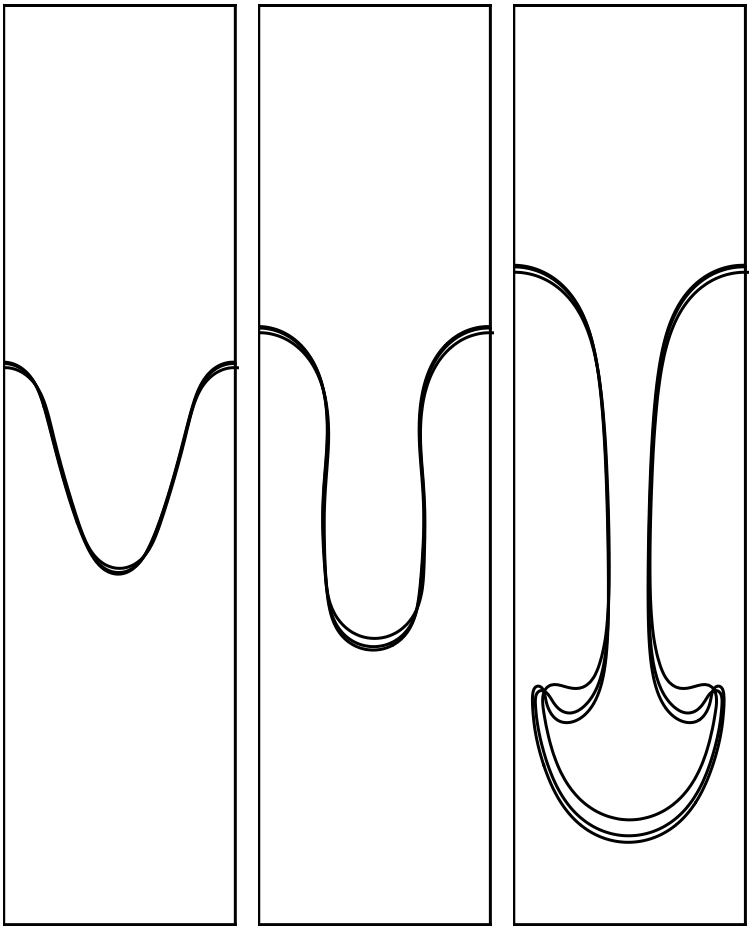

FIGURE 4. The shape of the interface in the Rayleigh-Taylor instability problem at $t = 1$ (left), $t = 5$ (middle), and $t = 10$ (right). Higher resolution simulations give deeper penetration. Simulations with 64×256, 128×512, and 256×1024 lattices are shown.

where $a_0 = 0.1L_x$. The density ratio ρ_h/ρ_l is 10, and the kinematic viscosity for both fluids is 0.0167. The normailzied surface tension coefficient S is 0.5, where

$$S = \frac{\sigma}{(\rho_h + \rho_l)(g\nu^4)^{1/3}}. \tag{3.10}$$

The gravity g is set such that the wave number of the intial perturbation is 0.35 in the unit of $(g/\nu^2)^{1/3}$. The time evolution of the interface shapes for different lattice sizes is shown in Fig. 4.

4. Conclusions

A lattice Boltzmann method for multiphase flows with large density ratios has been developed. One of origins of the large density ratio problem in the LB method is discussed.

It is found that the discrete operator corresponding to the LB dynamics does not exactly satisfy the chain rule of the derivative operator. This can result in significant errors when the density ratio between different phases is larger than 100. As an example, the error in the divergence-free constraint in incompressible flows is shown to be much larger than the truncation error in the LB method, $O(\mathrm{Ma}^2)$. To remedy this problem, a new formulation where the equilibrium function is expanded using the velocity rather than the momentum, as in the conventional LB method, is proposed. The continuity error in the new formulation is shown to be within the truncation error of the LB method. The new LB method is applicable to density ratios up to $O(1000)$.

Acknowledgment

Financial support by Honda R&D Co., Ltd. Fundamental Technology Research Center, is gratefully acknowledged.

REFERENCES

Benzi, R., Succi, S. & Vergassola, M. 1992 Thee lattice Boltzmann-equation - Theory and applications. *Phys. Reports* **222**, 145–197.

Chen, S. & Doolen, G. D. 1998 Lattice Boltzmann method for fluid flows. *Annu. Rev. Fluid Mech.* **30**, 329–364.

He, X., Zou, Q., Luo, L.-S. & Dembo, M. 1997 Analytic solutions of simple flows and analysis of nonslip boundary conditions for the lattice Boltzmann BGK model. *J. Stat. Phys.* **87**, 115–136.

Inamuro, T., Ogata, T., Tajima, S. & Konishi, N. 2004 A lattice Boltzmann method for incompressible two-phase flows with large density differences. *J. Comput. Phys.* **198**, 628–644.

Jacqmin, D. 1999 Calculation of two-phase Navier-Stokes flows using phase-field modeling. *J. Comput. Phys.* **155**, 96–127.

Lee, T. & Lin, C.-L. 2005 A stable discretization of the lattice Boltzmann equation for simulation of incompressible two-phase flows at large density ratio. *J. Comput. Phys.* **206**, 16–47.

van Leer, B. 1979 Towards the ultimate conservative difference scheme. v. a second-order sequel to Godunov's method. *J. Comp. Phys.* **32**, 101–136.

McNamara, G. R. & Zanetti, G. 1988 Use of the Boltzmann equation to simulate lattice-gas automata. *Phys. Rev. Lett.* **61**, 2332.

Pooley, C. M. & Furtado, K. 2008 Eliminating spurious velocities in the free-energy lattice Boltzmann method. *Phys. Rev. E* **77**, 046702.

Qian, Y. H., d'Humieres, D. & Lallemand, P. 1992 Lattice BGK models for Navier–Stokes equation. *Europhys. Lett.* **17**, 479–484.

Ricot, D., Marie, S., Sagaut, P. & Bailly, C. 2009 Lattice Boltzmann method with selective viscosity filter. *J. Comput. Phys.* **228**, 4478–4490.

Shan, X. & Chen, H. 1993 Lattice Boltzmann method for simulating flows with multiple phases and components. *Phys. Rev. E* **47**, 1815–1819.

Succi, S. 2001 *Lattice Boltzmann Equation for Fluid Dynamics and Beyond*. Clarendon Press.

Swift, M. R., Orlandini, E., Osborn, W. R. & Yeomans, J. M. 1996 Lattice Boltzmann simulation of liquid-gas nad binary fluid systems. *Phys. Rev. E* **54**, 5041.

Zheng, H. W., Shu, C. & Chew, Y. T. 2006 A lattice Boltzmann model for multiphase flows with large density ratio. *J. Comput. Phys.* **218**, 353–371.